Pergamon

Geochimica et Cosmochimica Acta, Vol. 66, No. 4, pp. 699–711, 2002

0016-7037/−1898 $22.00 + .00

PII S0016-7037(01)00799-2

Smyer H-chondrite impact-melt breccia and evidence for sulfur vaporization

ALAN E. RUBIN*

Institute of Geophysics and Planetary Physics, University of California, Los Angeles, CA 90095-1567, USA

(*Received October* 20, 2000; *accepted in revised form August* 22, 2001)

Abstract—Smyer is an H-chondrite impact-melt breccia containing ~20 vol% 0.5- to 13-mm-thick silicate-rich melt veins surrounding unmelted subrounded chondritic clasts up to 7 cm in maximum dimension. At the interface between some of the melt veins and chondritic clasts, there are troilite-rich regions consisting of unmelted, crushed 0.2- to 140-μm-size angular silicate grains and chondrule fragments surrounded by troilite and transected by thin troilite veins. Troilite fills every available fracture in the silicates, including some as thin as 0.1 μm. Little metallic Fe-Ni is present in these regions: the FeS/Fe modal ratio ranges from ~25:1 to ~500:1, far higher than the eutectic weight ratio of 7.5:1. The texture of these regions indicates that the sulfide formed from a fluid of very low viscosity. The moderately high viscosity (0.2 poise) and large surface tension of liquid FeS, its inability to wet silicate grain surfaces at low oxygen fugacities, and the supereutectic FeS/Fe ratios in the troilite-rich regions indicate that the fluid was a vapor. It seems likely that during the shock event that melted Smyer, many silicates adjacent to the melt veins were crushed. Upon release of shock pressure, some of the troilite evaporated and dissociated. Molecules of S_2 were transported and condensed into fractures and around tiny silicate grains; there, they combined with Fe from small adjacent metallic Fe-Ni grains to form troilite. The Ni content at the edges of some of these metal grains increased significantly; Co from these Ni-rich grains diffused into nearby kamacite. Impact-induced S volatilization may have played a major role in depleting the surface of 433 Eros (and other chondritic asteroids) in S. *Copyright © 2002 Elsevier Science Ltd*

1. INTRODUCTION

In most shocked ordinary chondrites (OC), troilite has been mobilized (e.g., Bennett and McSween, 1996) because of its high compressibility and because the Fe-FeS eutectic temperature of 988°C is locally exceeded during many shock events. Many OCs that have experienced equilibrium peak shock pressures above 10 to 20 GPa (i.e., shock stage ≥S3; Stöffler et al., 1991) exhibit silicate darkening in transmitted light (Rubin, 1992) caused by the dispersion of tiny metal and troilite blebs through the silicates. Many shocked OC contain fine-grained, rapidly solidified metal–troilite mixtures with dendritic or cellular textures (Scott, 1982). Some shocked OC contain large (>4 mm size) opaque nodules consisting mainly of metallic Fe-Ni, troilite, or both phases (e.g., Rubin, 1985, 1999; Widom et al., 1986).

Some OCs are impact-melt breccias. A few of these have been nearly completely melted—for example, the L chondrite PAT91501 (Mittlefehldt and Lindstrom, 2001) and the LL chondrite Y-74160 (Takeda et al., 1984). However, the majority of OC impact-melt breccias contain appreciable amounts of relict chondritic material—for example, Rose City, H5 (Mason and Wiik, 1966; Fruland, 1975), Cat Mountain, L5 (Kring et al., 1996), Chico, L6 (Bogard et al., 1995), Shaw, L6 (Taylor et al., 1979), Ramsdorf, "L7" (Yamaguchi et al., 1999), and Y-790143, LL6 (Sato et al., 1982). In many of the impact-melt breccias, troilite occurs in opaque shock veins along with metallic Fe-Ni. Within silicate-rich melt regions, troilite occurs in cellular and dendritic metal–troilite mixtures and as rinds on rounded metallic Fe-Ni blebs.

Metal veins and large metallic Fe-Ni nodules with fractionated refractory siderophile elements have been modeled as having formed by shock vaporization and fractional condensation of metal (Widom et al., 1986; Rubin, 1995, 1999). Because troilite is typically associated with metallic Fe-Ni in OC, troilite should also have been vaporized in some shocked OC. It seems plausible that the large troilite nodules in OC formed by shock-vaporization/condensation (Rubin, 1999). Olsen (1981) reported evidence for shock vaporization and vapor deposition of troilite and other phases. These phases occur as small euhedral grains lining the walls of vugs in OC fragmental breccias such as L5 Farmington.

Additional evidence for shock-vaporization of sulfide in the Smyer H-chondrite impact-melt breccia is described below. This 3273-g rock was found as a single stone in a cultivated field in Hockley County, Texas, in 1968 (Grady, 2000). In his brief description of Smyer, King (1979) noted its textural similarity to the Rose City and Myersville H-chondrite impact-melt breccias.

2. ANALYTICAL PROCEDURES

Six slabs of Smyer with a total surface area of ~600 cm^2 were examined visually. One 27-cm^2 slab was polished and examined microscopically in reflected light. Four thin sections of Smyer (LC 755 to LC 758) were examined microscopically in transmitted and reflected light. Point counting was performed in reflected light with an automated stage. The following densities were used for the conversion of vol% into wt%: silicate, 3.3; metallic Fe-Ni, 7.95; troilite, 4.67; and chromite, 4.7 g cm^{-3}. Sizes of constituents were determined microscopically with a calibrated reticle. Mineral analyses were conducted with the Cameca electron microprobe at the University of California, Los Angeles (UCLA), with natural and synthetic standards,

* (aerubin@ucla.edu).

20-s counting times, and ZAF and PAP corrections. Backscattered electron images were taken with the LEO 1430 SEM at UCLA. Transmitted and reflected light images were made with a digital camera attached to an Olympus BX60 petrographic stereomicroscope.

A 26-mg metal-sulfide nodule was removed from a Smyer slab with stainless steel dental tools and analyzed by instrumental neutron activation analysis (INAA) by use of the procedures of Willis and Wasson (1981). Standards included the Filomena and Coahuila IIAB iron meteorites and NBS 809B. Samples were counted four times over a period of 4 weeks. Gamma-ray peaks were determined by the SPECTRA program of Baedecker and Grossman (1989).

3. RESULTS

3.1. General Characteristic of OCs

Metamorphosed, unbrecciated OC consist mainly of recrystallized chondrules, coarse mafic silicate grains in the interchondrule matrix, and grains of metallic Fe-Ni, troilite, and chromite (e.g., fig. 2.1 of Dodd, 1981). Brecciated OC consist of angular clasts of OC material, in many cases embedded in a darker matrix containing fine-grained metal and sulfide (e.g., fig. 2.14 of McSween, 1999). OC impact-melt breccias contain moderately rounded clasts of OC material surrounded by veins or thick patches of solidified impact melt (e.g., Cat Mountain; fig. 1 of Kring et al., 1996); in some cases (e.g., Rose City), metallic Fe-Ni–rich veins surround the OC clasts (e.g., fig. 3 of Bogard, 1979).

3.2. Whole Rock

Smyer is an impact-melt breccia that resembles Rose City. Smyer consists of ~80 vol% subrounded unmelted chondritic clasts and ~20 vol% silicate-rich melt veins. Between some of the clasts and melt veins are troilite-rich regions consisting of angular silicate grains and chondrule fragments surrounded and transected by troilite. Each of these components is described below.

3.3. Unmelted Chondritic Clasts

Subrounded unmelted chondritic clasts are typically several centimeters in maximum dimension and range from ~0.1 to ~7 cm. A large unmelted clast (clast A) measured in thin section LC 755 has a modal composition of 80.1 wt% silicate, 14.1 wt% metallic Fe-Ni, 5.4 wt% troilite, and 0.4 wt% chromite (n = 3155 points; 228 mm^2). The metallic Fe-Ni abundance is within the range of H4-6 falls (13.2 to 21.2 wt%; Jarosewich, 1990) but lower than the mean value (17.8 wt%). The troilite abundance (5.4 wt%) is the same as the mean value in H4-6 falls (Jarosewich, 1990); and the chromite abundance (0.4 wt%) is within the H4-6 range (0.1 to 0.6 wt%; Keil, 1962).

The mean size of the metallic Fe-Ni grains (130 ± 110 μm; n = 100) measured in several clasts is close to the mean in H5 chondrites (120 ± 150 μm; table 2 of Rubin et al., 2001a). The mean size of troilite in the clasts (60 ± 40 μm; n = 100) is within uncertainty the same as that in H5 chondrites (75 ± 70 μm; table 2 of Rubin et al., 2001a).

Moderately recrystallized, albeit well-delineated, chondrules of all common textural types (porphyritic olivine, porphyritic olivine–pyroxene, porphyritic pyroxene, barred olivine, cryptocrystalline, radial pyroxene and granular olivine–pyroxene) are present in the clasts, consistent with petrologic type 5. Coarse isolated olivine grains in the clasts contain planar fractures and exhibit highly undulose to mosaic extinction, indicating that the clasts have been shocked to shock stage S4 (Stöffler et al., 1991). The clasts contain polycrystalline troilite, a few cellular metal–troilite mixtures and metal–troilite shock veins ranging up to 4 cm in length. The shock veins are typically 10 to 20 μm wide and consist of dark silicate glass surrounding numerous round and elliptical troilite blebs containing small (0.1 to 1 μm) metal spherules. The clasts exhibit extensive silicate darkening due mainly to the high abundance of thin troilite veins at the boundaries between fragmented silicate grains (Fig. 1). In some places, the opaque veins contain ~70 vol% 0.2- to 5-μm-size angular silicate grains surrounded by metal or troilite. In the troilite-rich regions of the veins, thin (0.1 to 1 μm thick) spidery veins of troilite transect adjacent silicate grains.

The clasts contain many coarse metal–troilite assemblages where massive grains of the two phases are adjacent (Fig. 2). In many cases, small (1 to 10 μm) irregular, blocky, and crescent-shaped troilite grains constitute ~5 to 20 vol% of the metal-rich portions of these assemblages. Large isolated metal grains generally do not contain small irregular troilite grains.

Also present in the clasts are a few 100- to 300-μm-size chromite-plagioclase assemblages consisting of 40 to 60 vol% euhedral to rounded 0.2- to 4-μm-size chromite grains (many intergrown with each other) embedded in plagioclase glass (e.g., Fig. 3). Similar chromite–plagioclase intergrowths occur in the H-chondrite breccias Portales Valley (Rubin et al., 2001a) and Zag (Rubin et al., 2001b). Some of the coarse (50 to 700-μm) metal grains in the clasts are surrounded by ~2-μm-thick rims of troilite. Thin veins of troilite extending from these rims cut across adjacent silicate grains.

The mean compositions of the silicates in the unmelted clasts (Table 1) are (in mol%): olivine (Fa18.8), low-Ca pyroxene (Fs16.5Wo1.5), diopside (Fs6.9Wo46.1), and plagioclase (Ab81.8Or5.3). These compositions are in the range of H-group chondrites: olivine Fa17.3-20.2 (Rubin, 1990); low-Ca pyroxene Fs15.7-18.1 (Gomes and Keil, 1980); diopside Fs5.7-7.0Wo~45 (Brearley and Jones, 1998); plagioclase Ab79.2-83.1Or5.2-7.7 (Van Schmus and Ribbe, 1968).

Metallic Fe-Ni grains in the clasts average 6.3 wt% Ni and 0.50 wt% Co (Table 2). These concentrations are within the established ranges of equilibrated H chondrites: 6.3 to 7.5% Ni and 0.44 to 0.51 wt% Co (table 3 of Rubin, 1990).

3.4. Silicate-Rich Melt Veins

The silicate-rich melt veins are typically 2 to 5 mm thick but range in thickness from 0.5 to 13 mm. The major constituent of the melt veins (~85 vol%) is a brown mesostasis that consists mainly of 2- to 10-μm-size intergrown angular mafic silicate grains surrounded by 0.3- to 2-μm-thick patches of silico-feldspathic glass (Fig. 4; Table 1). Some of the mafic silicate grains in the melt appear to have nucleated at the surface of larger (30- to 150-μm-size) mosaicized olivine grains or 10- to

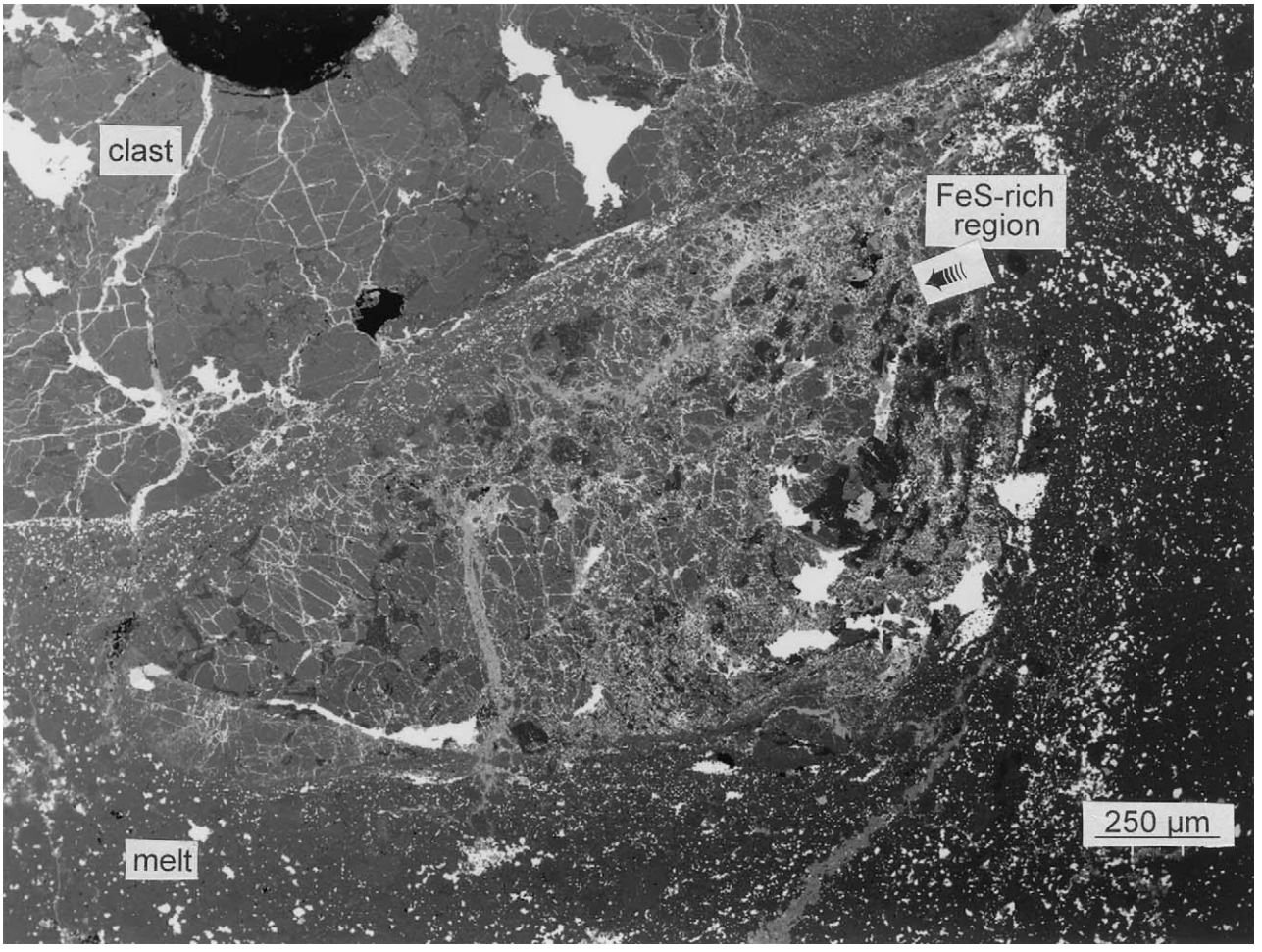

Fig. 1. Portion of Smyer showing an unmelted chondritic clast (medium gray; upper left) transected by numerous thin veins of troilite (white). Also present in the clast are a few large metallic Fe-Ni grains (white). The black semicircle at upper left is part of a bubble in the thin-section epoxy. A clamshell-shaped troilite-rich region occurs in the center of the image, separated from the clast by a thin channel of silicate-rich melt containing numerous tiny metal blebs. The troilite-rich region contains shattered silicate grains transected and surrounded by troilite. Also present is a thin vein of limonite (light gray; left of center), a product of terrestrial weathering. Silicate-rich melt also occurs below and at the sides of the troilite-rich region (back-scattered electron image).

700-μm-size chondrule fragments. Many of the olivine grains exhibit silicate darkening due to the dispersion of numerous 0.2- to 2-μm-size grains of metal, chromite, and troilite inside them. The compositions of the larger silicate grains (Fig. 4) within the melt regions (olivine Fa18.4; low-Ca pyroxene Fs16.5Wo1.3; plagioclase Ab84.4Or4.1; Table 1) are very similar to those in the unmelted chondritic clasts, suggesting that they are relict grains that survived impact melting.

Also present within the melt veins are 10 to 15 vol% subangular to rounded cellular metal–troilite intergrowths (with 9- to 22-μm-wide metal cells; mean width, 15 μm) (e.g., Fig. 5), numerous tiny (0.1 to 1 μm) metal particles (Fig. 5), rare 1- to 4-mm-size metal nodules, and rare 5-μm-size euhedral to subhedral chromite grains (Fig. 5).

The number of tiny metal particles in the melt veins increases about fourfold within 300 μm of the edge of some of the unmelted silicate clasts (Fig. 5), giving the edges a much darker appearance in transmitted light. Rimming the unmelted clasts, at the interface between the clasts and the silicate-rich melt, are 10- to 120-μm-thick, elongated, metal-rich cellular metal–troilite assemblages, troilite-poor metallic Fe-Ni veins, or both. In some cases, the metallic Fe-Ni veins occur within the silicate-rich melt and not at the edge of a chondritic clast (Fig. 2). Associated with some of the metal veins are distinctive troilite-rich regions (Fig. 2) as described below.

3.5. Troilite-Rich Regions

Troilite-rich regions (Figs. 6 to 8) typically consist of 50 to 70 vol% troilite, 30 to 50 vol% silicate, $<$2 vol% metallic Fe-Ni, and trace amounts of chromite; some regions contain a few 100- to 200-μm-size metal grains separated by troilite-rich patches up to 1.8 mm in maximum dimension that contain only trace amounts of metallic Fe-Ni. Troilite-rich regions occur in between some of the unmelted silicate clasts and silicate-rich melt veins. The regions contain unmelted, angular silicate grains (olivine, low-Ca pyroxene, and plagioclase) as small as 0.2 μm, angular chondrule fragments ranging up to 140 μm,

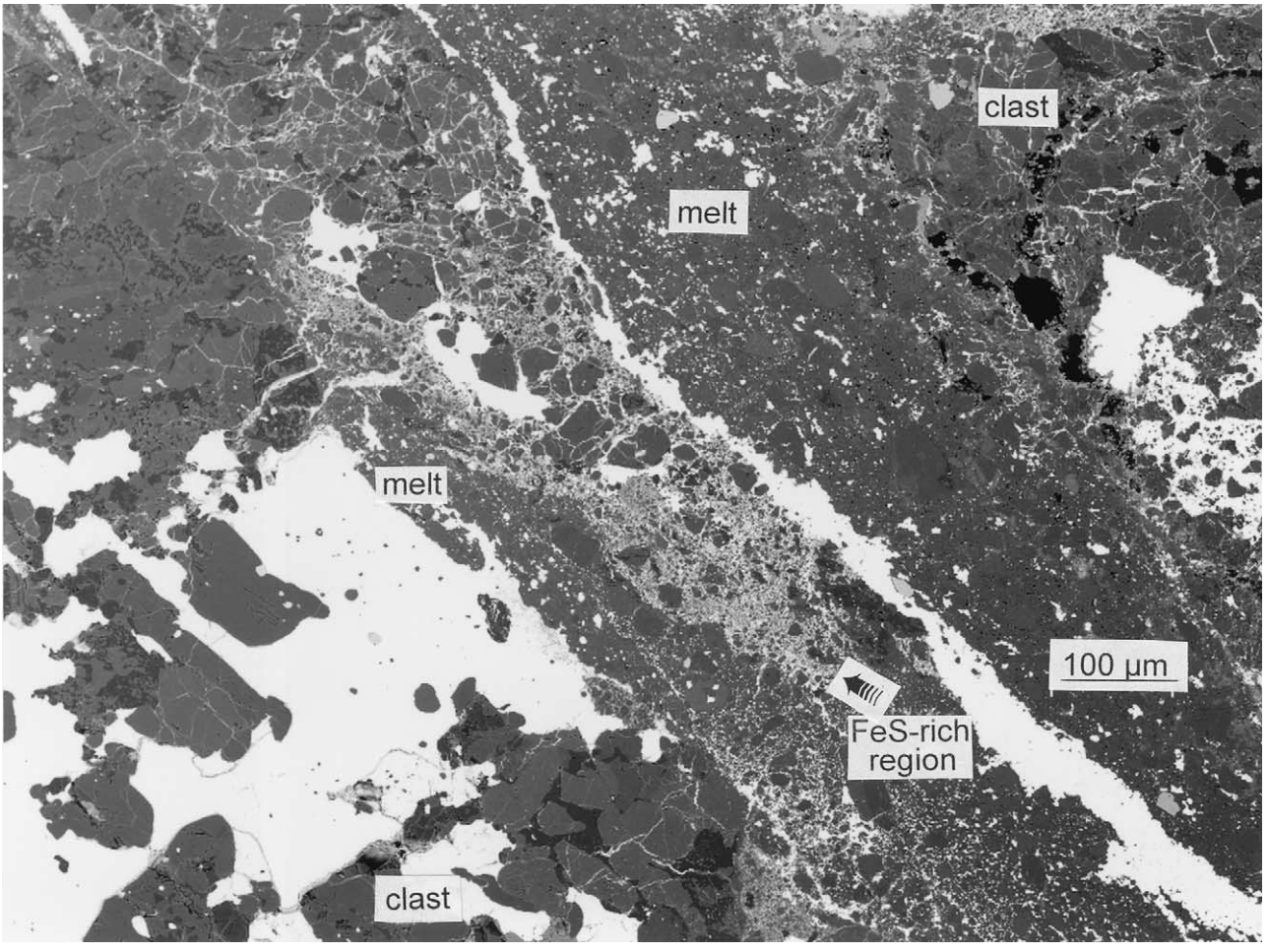

Fig. 2. Edge of unmelted chondritic clast (lower left) containing large metal–troilite assemblage (white) and included silicate grains (gray). Immediately above and to the right of the clast is a layer of silicate-rich melt, followed by a small troilite-rich region, a thin metallic Fe-Ni vein (white), a thick channel of silicate-rich melt, and, at upper right, another unmelted chondritic clast containing a coarse metal grain (back-scattered electron image).

and a few patches of glass (with the composition of a Na-depleted mixture of plagioclase, diopside, and olivine and/or low-Ca pyroxene) (Table 1).

The larger silicate grains have been crushed and are surrounded by troilite and transected by numerous 0.1- to 1-μm-thick troilite veins, which constitute 2 to 5 vol% of the large silicate grains (Fig. 6). The small mafic silicate grains in these regions are all surrounded by troilite and show normal igneous zoning—that is, their edges have higher FeO/MgO ratios than their cores. Very little metallic Fe-Ni is present; the FeS/Fe volume ratios in these regions range from ~25:1 to ~500:1 (Fig. 7). The metal grains that are present in the troilite-rich regions of Smyer contain a few 1- to 2-μm-size patches of troilite at their margins connected to small adjacent silicate grain fragments (Fig. 8). Sulfide grains in the troilite-rich regions range in composition from pyrrhotite with atomic Fe/S ratios of 0.93 to stoichiometric troilite (Table 2). None of the sulfide grains contain detectable concentrations of Co.

Most kamacite grains in the troilite-rich regions have normal Ni and Co concentrations (6.3 to 6.8 wt% Ni and 0.44 to 0.51 wt% Co), typical of H-group chondrites (Rubin, 1990) and similar to those of the metal grains in the chondritic clasts (Table 2). However, some of the kamacite grains in the troilite-rich regions have Co concentrations (0.53 to 0.55 wt%), slightly higher than the typical H-chondrite range (0.44 to 0.51 wt%; Rubin, 1990). In addition, some grains are enriched in Fe; their Ni contents (5.0 to 6.2 wt%) are below those of kamacite grains in the chondritic clasts (6.3 wt%) and below kamacite in equilibrated H chondrites (6.3 to 7.5 wt%; Rubin, 1990). A few metallic Fe-Ni grains in the troilite-rich clasts are significantly enriched in Ni and depleted in Co, particularly near their edges (Table 2). For example, grain 24 (20 μm in size) contains 22.2 wt% Ni and 0.38 wt% Co at its center and 32.7 wt% Ni and 0.36 wt% Co at its edge. Grain 8 (100 μm) from a different troilite-rich region is also compositionally zoned: it contains 22.2 wt% Ni and 0.17 wt% Co at its center and 28.5 wt% Ni and 0.10 wt% Co at its edge.

3.6. Metal-Sulfide Nodule

A 26-mg opaque nodule, removed from the edge of a silicate melt region, consists of kamacite and minor troilite. Its bulk

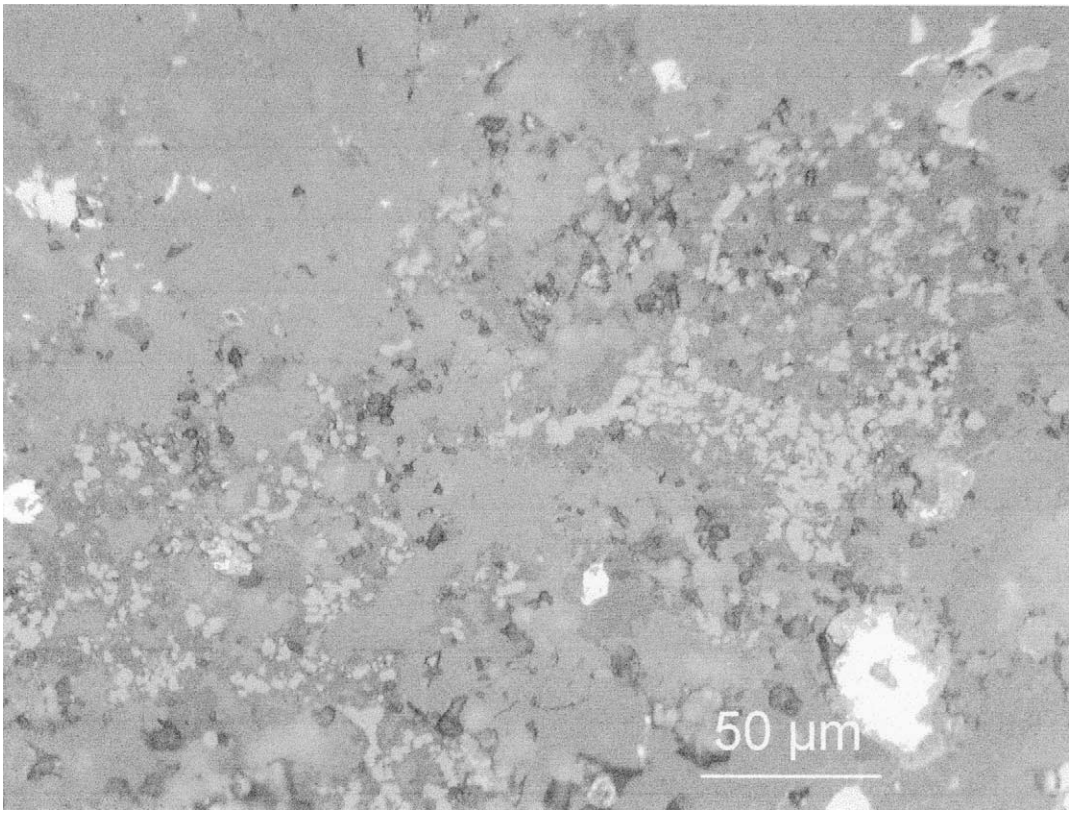

Fig. 3. Irregular, discontinuous chromite–plagioclase assemblage consisting of small euhedral, subhedral, and anhedral grains of chromite (light gray) embedded in glass of plagioclase composition (dark gray). The assemblage occurs within an unmelted chondritic clast consisting mainly of silicate (medium gray) and grains of metallic Fe-Ni (white) (reflected light).

composition (Table 3; Fig. 9) shows that many elements (Re, Os, Ir, Ru, Ni, Co, Fe, Au) are within ~20% of the abundances of normal H-chondrite metal as represented by metal from the Jilin H5 chondrite (Kong et al., 1998). Because of potential sampling difficulties with Jilin bulk metal, these elements are probably not significantly different in the Smyer nodule and Jilin metal. Elements outside the uncertainty range include W (depleted by 28%), Mo (enriched by 43%), As (depleted by 35%), Cu (enriched by 103%), Ga (enriched by 54%), and Sb (depleted by 37%).

4. DISCUSSION

4.1. Formation of the Smyer Impact-Melt Breccia

The shock effects exhibited by the chondritic clasts and the presence of a silicate melt in Smyer indicate that an impact

Table 1. Compositions (wt%) of silicate phases in chondritic clasts and silicate-rich melt regions.

	Phases in chondritic clasts				Phases in silicate-rich melt regions			
Parameter	Olivine	Low-Ca pyx	Diopside	Plagioclase	Olivine	Low-Ca pyx	Plagioclase[a]	Glass[b]
No. of grains	2	2	1	1	5	7	1	4
SiO_2	39.1	56.2	54.8	65.9	39.3	56.8	(65)	67.8
Al_2O_3	<0.04	0.16	0.65	21.6	0.04	0.24	(22)	9.3
FeO	17.5	11.0	4.3	0.47	17.2	11.0	(0.5)	6.5
MnO	0.48	0.47	0.28	<0.04	0.45	0.49	<0.04	0.22
MgO	42.5	30.7	16.4	<0.04	42.8	30.8	(<0.04)	6.8
CaO	0.04	0.80	22.4	2.5	0.08	0.68	2.2	8.6
Na_2O	<0.04	<0.04	0.60	8.8	<0.04	<0.04	8.9	0.44
K_2O	<0.04	<0.04	<0.04	0.87	<0.04	<0.04	0.66	0.40
Total	99.6	99.3	99.4	100.1	99.9	100.0	99.3	100.1
End member	Fa18.8	Fs16.5	Fs6.9	Ab81.8	Fa18.4	Fs16.5	Ab84.4	
		Wo1.5	Wo46.1	Or5.3		Wo1.3	Or4.1	

[a] Numbers in parentheses are adjusted to correct for electron beam overlap of adjacent mafic silicate grains.
[b] Four patches of glass, normalized to 100 wt%; the original total was 95.6 wt% due to pores and holes.

Table 2. Compositions (wt%) of metallic Fe-Ni in different regions of Smyer.

Location	Clasts	opaque veins	FeS-rich regions	H chondrite kamacite				
Kamacite								
No. of grains	3	4	7					
Fe	92.8	92.3	92.4	92.6[a]				
Ni	6.3	6.2	6.2	6.9				
Co	0.50	0.48	0.48	0.47				
Total	99.6	99.0	99.1	100.0				
Selected analyses of Ni-rich metal grains in FeS-rich regions								
Grain number	24		33		6		8	
Grain radius	13 μm		18 μm		18 μm		24 μm	
Location	center	edge	center	edge	center	edge	center	edge
Fe	76.4	66.2	74.9	72.7	95.9	83.6	78.3	71.9
Ni	22.2	32.7	23.5	26.7	4.2	16.8	22.2	28.5
Co	0.38	0.36	0.30	0.40	0.50	0.38	0.17	0.10
Total	99.0	99.3	98.7	99.8	100.6	100.8	100.7	100.5
Sulfide in FeS-rich regions								
Mineral	po[b]	po	troilite					
Grain number	1	2	3					
Fe	61.4	61.2	62.2					
Ni	$<$0.04	$<$0.04	0.20					
Co	$<$0.04	$<$0.04	$<$0.04					
S	37.7	36.2	36.1					
Cr	0.19	0.15	0.40					
Total	99.3	97.6	98.9					
Atomic Fe/S	0.93	0.97	0.99					

[a] Fe calculated by difference.
[b] po = pyrrhotite.

event caused bulk melting of chondritic material in Smyer's region of the H-chondrite asteroid. The structure of Smyer resembles that of many other OC impact-melt breccias in containing moderately rounded chondritic clasts surrounded by melt. Such breccias include Rose City (e.g., Bogard, 1979; Rubin, 1985), Cat Mountain (Kring et al., 1996), Chico (e.g., Bogard et al., 1995), Myersville (King, 1979), and Madrid (Casanova et al., 1990). Immediately after the impact events, each of these rocks was composed of a mush consisting mainly of molten silicate, immiscible metal-sulfide droplets, and relict (i.e., unmelted) silicate grains and chondrule fragments. The silicate darkening evident in some of the relict grains in Smyer indicate that these grains were significantly shocked (cf. Rubin, 1992). The temperatures of these grains must have risen briefly above the Fe-FeS eutectic temperature of 988°C. Otherwise, nearby metal and sulfide would not have melted and migrated through fractures in the silicates to cause the evident silicate darkening (Rubin, 1992).

The fine-grain size of the phenocrysts within the silicate melt and the retention of relict grains indicate that the silicate melt cooled quickly, most likely by conduction via contact with adjacent cold chondritic clasts. Overgrowths on some of the relict grains resulted from the nucleation and epitaxial growth of mafic silicate grains from the melt. The rock must have been heated to at least 1150°C, approximately the solidus temperature of an H chondrite (Jurewicz et al., 1993); it is possible that the rock was heated to a temperature several hundred degrees higher. As the temperature of the melt cooled from $\geq$1150 to $<$988°C, the metal-sulfide droplets quenched into cellular metal grains surrounded by troilite.

The fourfold increase in the number of tiny metal particles within 300 μm of the edge of some of the unmelted silicate clasts (e.g., Fig. 5) probably resulted from trapping of the metal-sulfide droplets near the sides of the melt channel where the melt was cooler, more viscous, and slower moving due to the proximity of the cold relict chondritic clasts. The shock event that formed the silicate-rich melt also shocked the chondritic clasts, created chromite-plagioclase intergrowths (e.g., Ashworth, 1985), crushed many adjacent silicate grains, and vaporized troilite near the silicate melt.

4.2. Formation of the Metal-Sulfide Nodule

The metal-sulfide nodule probably formed in the aftermath of the impact event by separation of a metal-sulfide droplet from the immiscible silicate melt. The compositional differences between the nodule and bulk metal (Table 3; Fig. 9) reflect the nodule's origin. The high Se and Cu in the nodule result from enrichment of the nodule in sulfide relative to bulk Jilin metal. The group VIB element Se has a strong chemical affinity for S and partitions into sulfide (e.g., Mason and Graham, 1970); Cu is moderately chalcophile and partitions into troilite (e.g., table 3 of Widom et al., 1986) and taenite (Mason and Graham, 1970; Kong et al., 1998) relative to bulk metal.

Gallium is enriched in taenite relative to bulk metal (Rambaldi and Cendales, 1979; Kong et al., 1998); thus, its high abundance in the kamacite-rich nodule in Smyer cannot be due to partitioning from taenite into kamacite. However, Chou and Cohen (1973) found that in highly shocked OC, lithophile Ga is reduced from silicates and partitions into metal. This process probably also operated in Smyer. Kong et al. (1998) found that W, As, and Sb partition into taenite relative to bulk metal. This

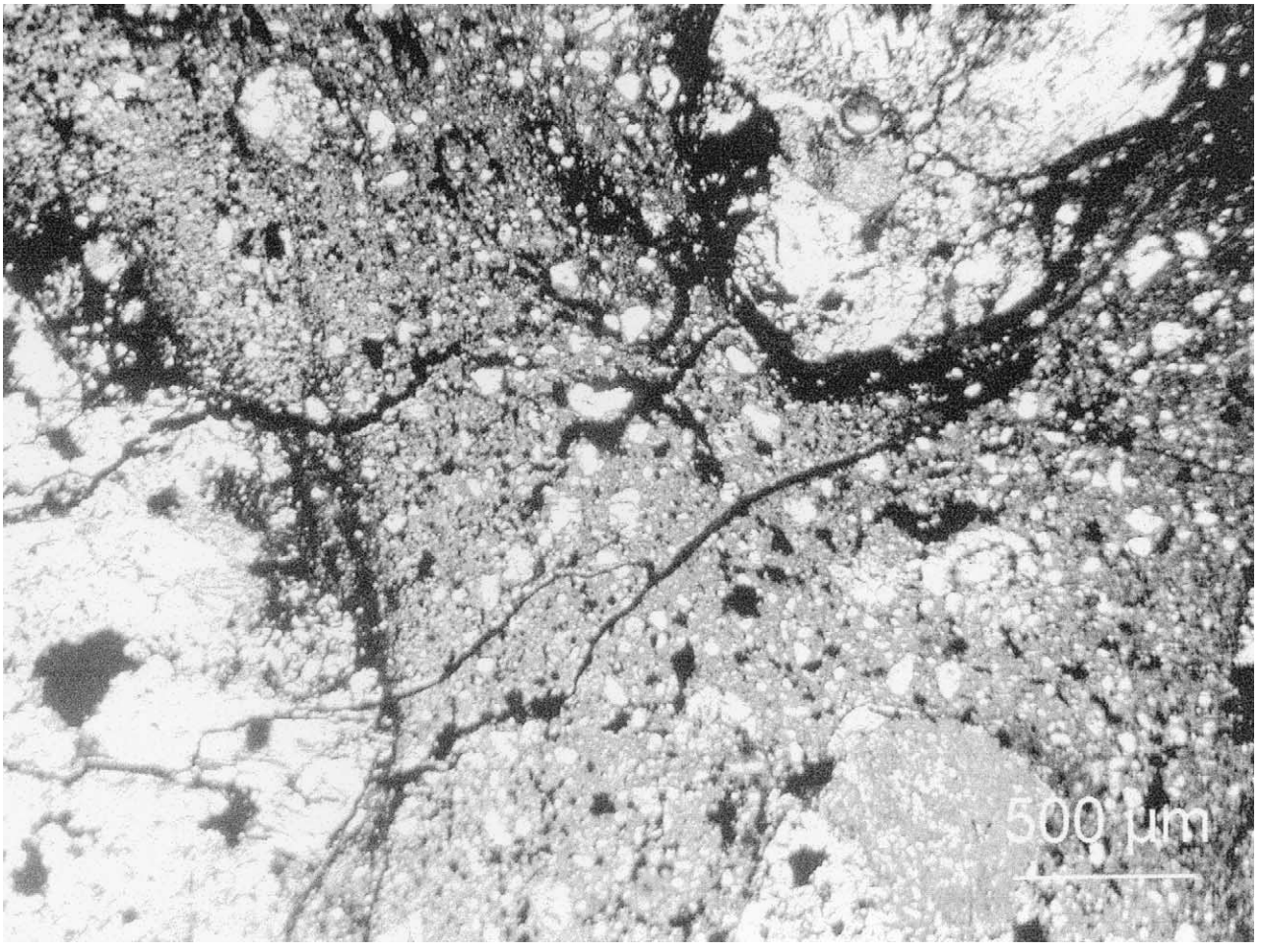

Fig. 4. Silicate-rich melt vein (center) separating unmelted chondritic clasts at top right and lower left. The melt contains numerous small mafic silicate grains and chondrule fragments (white) and opaque assemblages of metallic Fe-Ni and troilite (black). A few branching veins of limonite (black) due to terrestrial weathering cut across the image from upper right to lower left. High concentrations of metal and troilite at the clast boundaries appear as black rims around the clasts (transmitted light).

accounts for the depletions of W, As and Sb in the kamacite-rich nodule in Smyer.

The one unresolved compositional anomaly of the Smyer metal nodule is its 43% enrichment in Mo relative to bulk metal. Molybdenum partitions slightly into taenite relative to bulk metal (fig. 3 of Kong et al., 1998); its concentration in troilite is approximately one-third to one-half that of bulk metal (Mason and Graham, 1970). It seems plausible that the presence of significant troilite in the Smyer nodule accounts for the Mo enrichment.

4.3. Formation of Troilite-Rich Regions

There are several reasons why it is likely that the troilite in the troilite-rich regions formed by vapor deposition and not by crystallization from a melt.

(1) The silicate grains surrounded by the troilite have not been melted (Fig. 6); they are angular fragments that exhibit undulose to mosaic extinction. They would have melted if the temperature had been more than ~1150°C (i.e., near the H-chondrite solidus temperature; Jurewicz et al., 1993) and if sufficient time had been available for heat transfer from the melt. Because individual mineral fragments are present in these regions, their melting temperatures (which range from ~1130°C for $Ab_{84}Or_4$ plagioclase to ~1690°C for Fa_{18} olivine) may be more relevant than that of the bulk rock. Therefore, if the temperature had been <1130°C, it might also have been lower than the Fe-FeS eutectic temperature of 988°C (although this has not been established). If so, then the troilite in these regions could not have melted. Although this is a weak argument against the presence of molten FeS in these regions, the evidence is consistent with the deposition of sulfur from a vapor.

(2) The FeS/Fe modal abundance ratio in these regions (Figs. 6 and 7) far exceeds the eutectic weight ratio of 7.5:1 (e.g., Brandes and Brook, 1992). Such a high abundance of troilite could not have been produced by equilibrium melting. Because shock melting is not an equilibrium process, we need to examine the FeS/Fe ratio in materials that have been shock melted. Such material includes rapidly solidified metal–troilite mixtures (Scott, 1982), melt pockets (e.g., Dodd and Jarosewich,

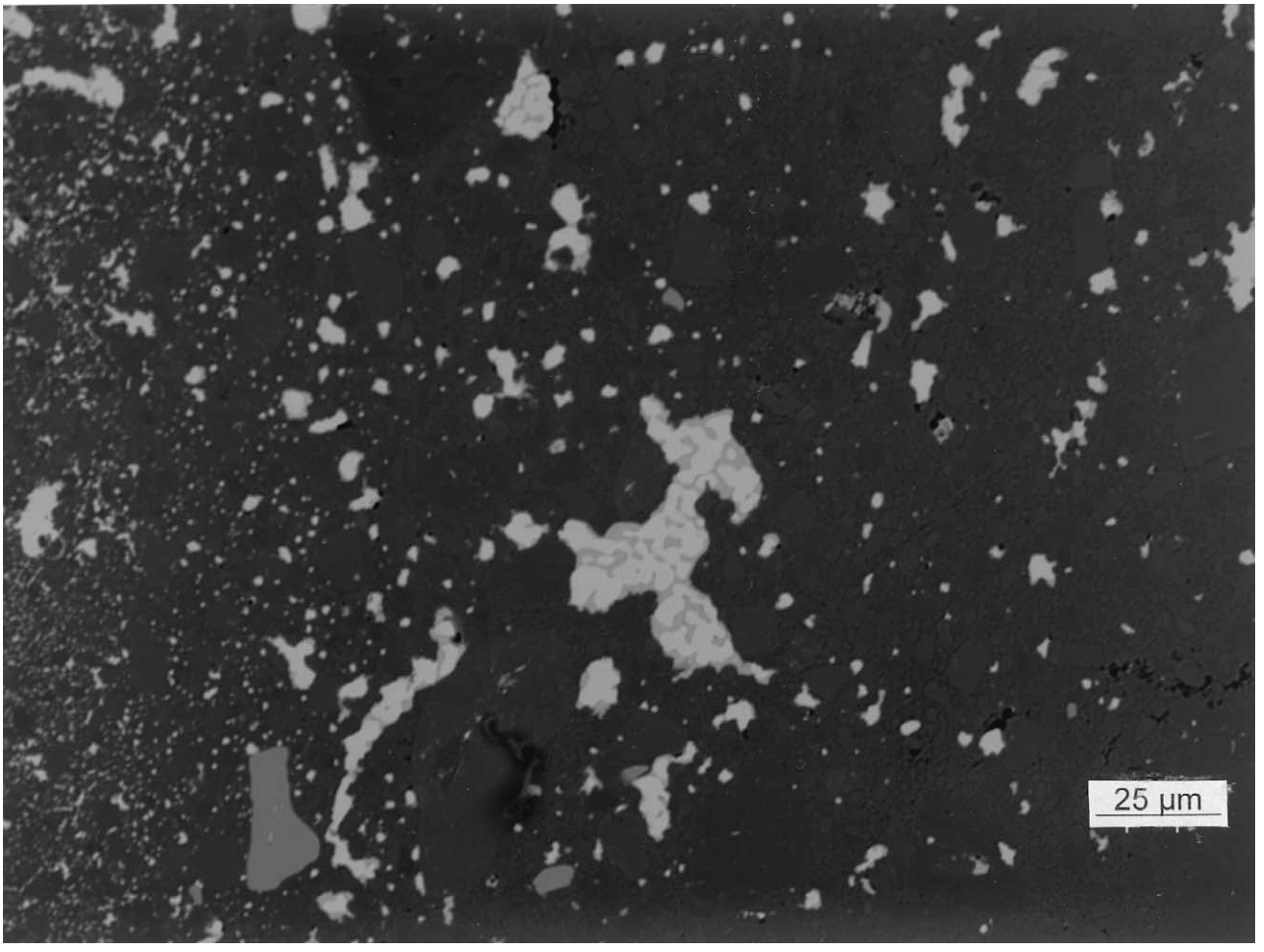

Fig. 5. Irregular cellular metal–troilite assemblage (white with light gray patches) within a channel of silicate-rich melt (very dark gray). Subhedral chromite grains (medium gray) occur within the melt at lower left and bottom center. The abundance of tiny metal blebs (white) increases significantly toward a chondritic clast (not shown) at left (back-scattered electron image).

1979, 1982) and impact-melt-rock clasts (e.g., Rubin, 1985, and references therein).

Although Scott (1982) does not list the FeS/Fe ratios of the metal–troilite mixtures he studied, the near extremes appear in his figures 3 and 4. From these photomicrographs, I determined the approximate FeS/Fe volume range of the metal–troilite mixtures to be 0.1 to 0.7. This corresponds to an approximate weight ratio range of 0.07 to 0.40. Dodd and Jarosewich (1982) analyzed melt pocket glasses in L6 chondrites; their data show an FeS/Fe weight ratio range of 0.02 to 2.9.

Most impact melt-rock clasts are highly depleted in metal and troilite; these phases are lost as immiscible liquids during impact melting. However, Wilkening (1978) described a metal–troilite nodule in Tysnes Island that is incompletely separated from an adjacent silicate melt rock. It is clear that the opaque nodule formed from a melt. From Wilkening's data, I calculate an FeS/Fe weight ratio of 0.28. Thus, materials produced by equilibrium or shock melting do not in general appear to have FeS/Fe ratios that significantly exceed the eutectic ratio of 7.5:1. This suggests that the troilite-rich regions in Smyer were not formed from a melt.

(3) The rare metal grains in the troilite-rich regions (e.g., Fig. 8) lack the typical igneous metal–troilite textures (i.e., troilite partly or completely rimming spherical or ellipsoidal metal blebs) observed in low-FeO chondrules (Rubin et al., 1999) or in metal-bearing basaltic-andesitic rocks from Disko Island, West Greenland (Klöck, 1986). Furthermore, the rare metal grains in the troilite-rich regions contain inclusions of shattered silicate surrounded by troilite (Fig. 8). If the troilite had been molten, the metal would probably also have been molten and would have formed a recognizably igneous metal–troilite intergrowth upon cooling.

(4) Troilite fills every available tiny fracture (including some as thin as 0.1 μm) in the crushed silicate grains (Fig. 6), texturally indicative of a low-viscosity S-rich fluid and consistent with condensation of S_2 from a vapor. It is unlikely that there would have been sufficient time during the pressure release stage for molten FeS to penetrate numerous very narrow fractures.

The physical properties of FeS melts mitigate against molten FeS being responsible for filling the narrow fractures in silicate grains. The viscosity η of molten FeS is 0.02 Pa-s (0.2 poise)

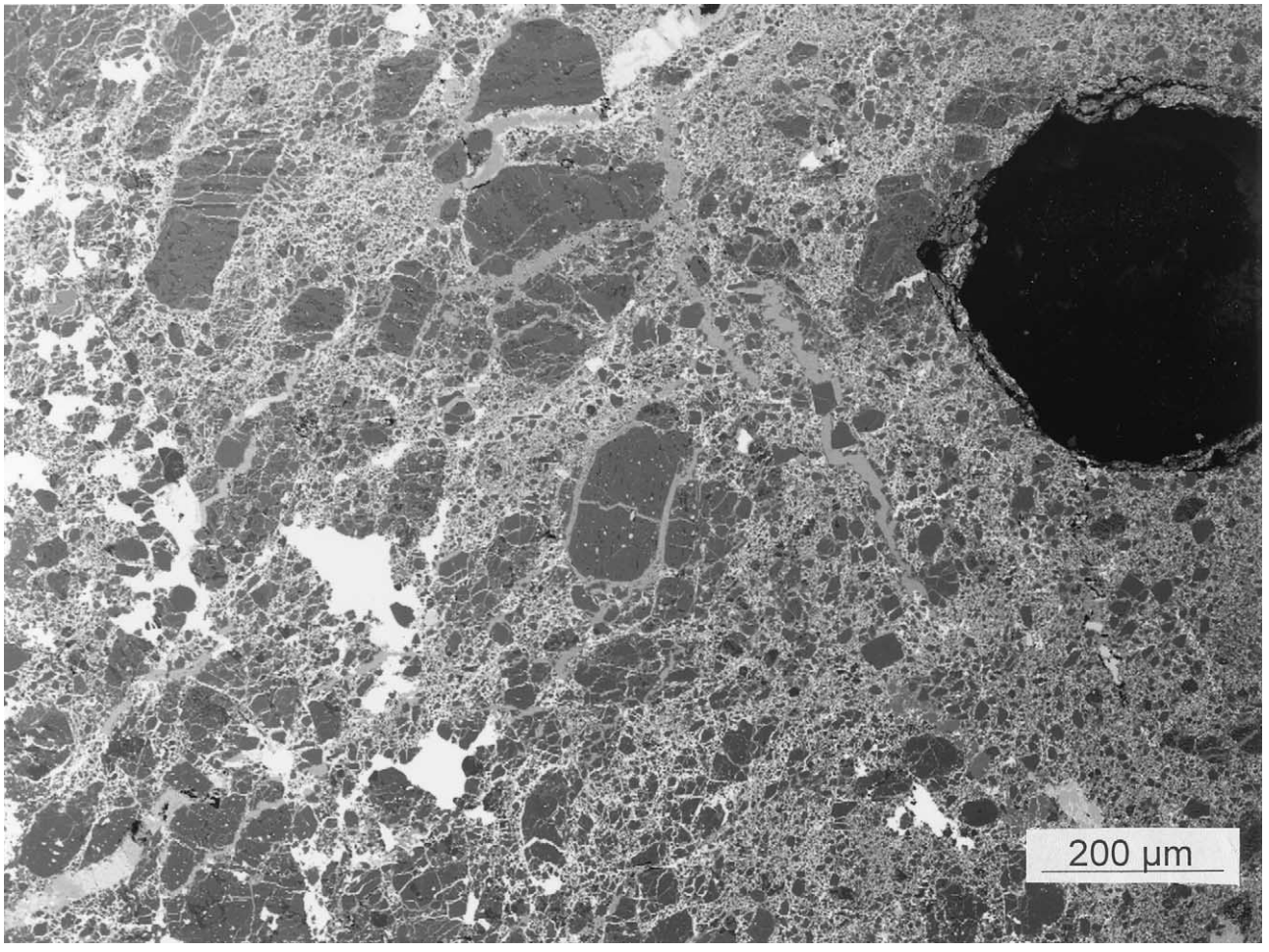

Fig. 6. A troilite-rich region in Smyer containing numerous shattered silicate grains (dark gray) transected and surrounded by troilite (very light gray to white). A bubble (black) in the epoxy of the thin section occurs at right. Also present in the troilite-rich region are small metal grains (white) that contain and are surrounded by silicate-troilite patches. Minor limonite (light gray) due to terrestrial weathering is also present around some of the silicate grains (back-scattered electron image).

at 1450°C and varies little with pressure (Dobson et al., 2000). Although this value is 30 times lower than the median value of melts of Apollo 11 igneous rocks at 1400°C (6 poises) (Weill et al., 1971), it is still 20 times greater than that of water at 20°C (0.01 poise). Also inconsistent with the penetration of the silicate cracks in Smyer by molten FeS are the experimental results of de Bremond d'Ars et al. (2001) showing that sulfide droplets have a large surface tension and do not coalesce during transport. The large surface tension of molten FeS diminishes the chances that it could fill narrow fractures. A related result was obtained by Rose and Brenan (2001) who found that molten sulfide lacking ≥15 wt% Cu, Co, or Ni does not significantly wet the surface of forsteritic olivine grains at 1300°C at low oxygen fugacities ($fO_2 \leq 10^{-9}$). This property also makes it likely that the FeS filling the narrow fractures in the silicates of the troilite-rich regions was not emplaced as a liquid.

I thus infer that during the shock event that melted portions of Smyer, many silicates adjacent to the melt regions were crushed. As the shock pressure was released, some of the troilite evaporated, releasing S_2 vapor. The S_2 condensed into fractures and around tiny silicate grains (i.e., places with high surface-area/volume ratios) and combined with Fe scavenged from adjacent grains of metallic Fe-Ni. In some cases, insufficient amounts of Fe were acquired and pyrrhotite formed with atomic Fe/S ratios as low as 0.93. The Ni contents of the metal grains that supplied the Fe to the sulfide increased significantly (particularly at their edges), in one case, increasing from 4.2 to 16.8 wt% over a distance of 18 μm (Table 2). The Co contents of the Ni-rich metal grains decreased from ~0.5 wt% to ~0.1 to 0.4 wt% as Co diffused into nearby kamacite grains, accounting for their slight Co enrichment. Some of the kamacite grains have low Ni contents (as low as 5.0 wt%), and, consequently, high Fe contents. Their relative enrichments in Fe may have been caused by acquisition of residual Fe from FeS after sulfur evaporated.

This scenario has significant experimental support. Lauretta (1997) heated a pressed pellet containing a mixture of metal, sulfide and silicate (in LL-chondrite proportions) in an evacuated silica tube inside a furnace that was flushed with N_2 to retard oxygen diffusion through the tube. Some charges were heated to 900°C; even though this is below the Fe-FeS eutectic

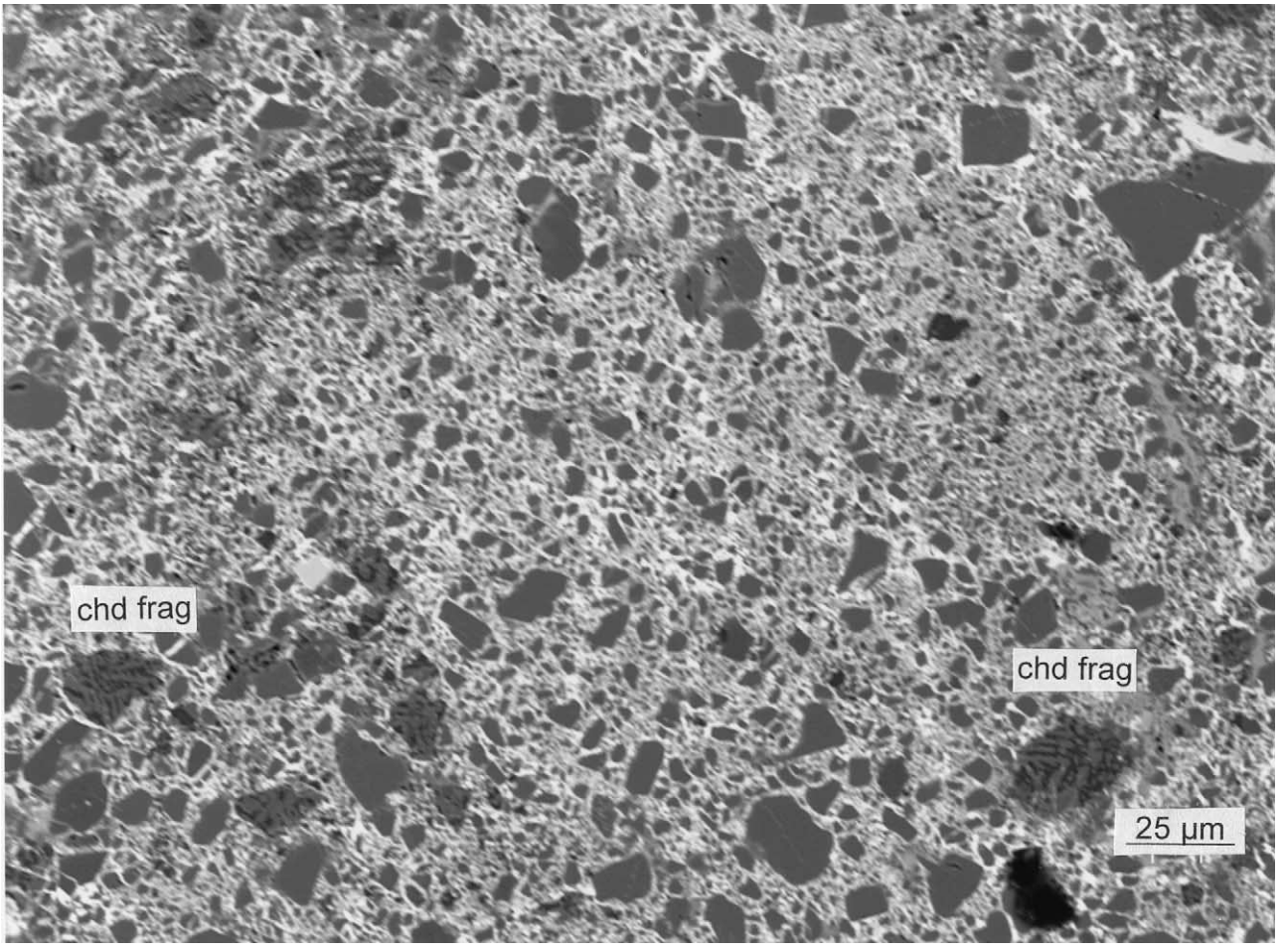

Fig. 7. Troilite-rich region showing numerous silicate grain fragments (dark gray) transected and surrounded by troilite (white). Small chondrule fragments (chd frag) (dark gray with black lines) occur at lower right and at left (back-scattered electron image).

temperature of 988°C, the sulfide in the charges evaporated, releasing S_2 vapor. This vapor was transported a short distance to a metal grain where S_2 molecules were adsorbed and dissociated into S atoms that reacted with Fe to form FeS.

The newly formed troilite extends away from the metal grain and interpenetrates adjacent silicate. The occurrence of sulfide within pore spaces of metal grains that were initially FeS-free indicates that sulfur vapor transport occurred (Lauretta et al., 1997). Charges heated to 900°C for 2 weeks show pronounced Ni enhancements in their metal grains within ~10 μm of the interface with sulfide: metal compositions vary from 6.4 wt% Ni in the original metal to a maximum of 9.5 wt% Ni in the resulting (presumably martensitic) metal phase at the edge (i.e., at the metal-sulfide boundary). Cobalt increases in this zone from 0.3 wt% in the original metal to 0.4 to 0.6 wt% in the martensite at the edge. In the 900°C experiment, sulfide rims around metal grains have grown large enough to incorporate adjacent silicate grains (Lauretta et al., 1997).

The major difference between these experimental results and the metal grains within the troilite-rich regions in Smyer is that the metal in the experimental charge acquired less Ni and more Co. The lower Ni concentration in the metal in the experiment probably resulted from the greater abundance of metal from which the sulfide could scavenge Fe. The higher Co in the experimental metal reflects the fact that the metal was transformed into the distorted body-centered cubic (α_2) structure, which can readily accommodate Co. In contrast, the metal in Smyer seems to have been transformed into taenite, a phase that accommodates less Co than kamacite. As indicated by D. Lauretta (personal communication), differences between the experimental results and meteoritic assemblages could also have resulted from differences in temperatures of formation, reaction kinetics and sulfur fugacity.

4.4. Impact Volatilization of S on Asteroids

Troilite-rich regions occur in several H-chondrite breccias: Smyer (this study), Myersville (Rubin, unpublished data), Zag (Rubin et al., 2001b), and Rose City (Rubin, unpublished data). This suggests that impact-vaporization of sulfide was a relatively common process on OC asteroids. Although S_2 condensed in these breccias after vaporization, some S_2 could have been lost, particularly from rocks near the surface of their parent bodies. This is consistent with the low bulk FeS abundance of Ramsdorf (an L-chondrite fall impact-melt rock; Yamaguchi et al., 1999), relative to that of mean L-chondrite

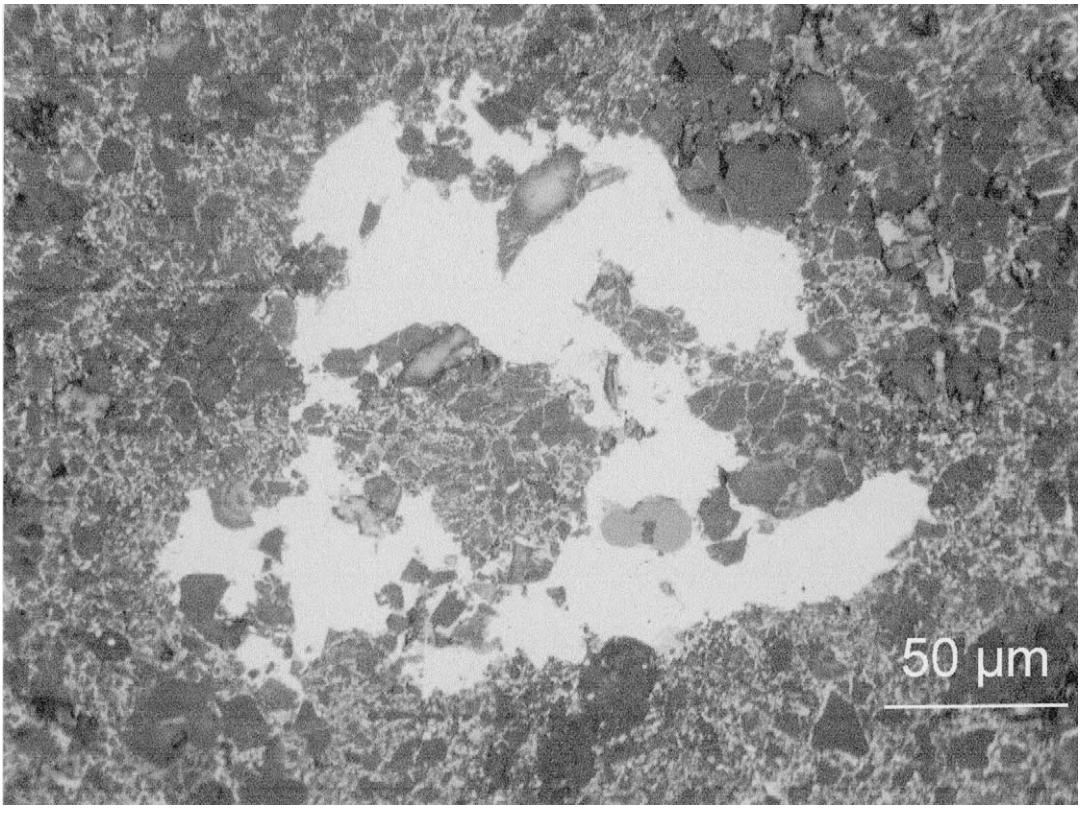

Fig. 8. Metallic Fe-Ni grain (white) in the middle of a troilite-rich region. The metal grain contains patches of silicate-troilite assemblages (dark gray surrounded by thin light gray lines) identical to those that occur outside the metal grain. Thin patches of troilite (light gray) occur in a few places at the sides of the metal grain. A small chromite grain (medium gray, right of center) partially surrounded by 1-μm-thick troilite rinds is also present in the metal (reflected light).

falls (3.87 wt% FeS vs. 5.76 $\pm$ 0.80 wt%; Jarosewich, 1990). Although it is possible that the low abundance of FeS in the Ramsdorf analysis is an artifact of unrepresentative sampling, it seems at least equally likely that the low FeS abundance is real and results from evaporation of troilite during an impact event. Such a possibility is supported by the occurrence of vesicles associated with troilite in the melt fractions of the Cat Mountain L-chondrite (Kring et al., 1996) and Y-790964 LL-chondrite (Miyamoto et al., 1984) impact-melt breccias. Some S was volatilized in these rocks during impact events.

I have argued that S is mobilized by impact vaporization in centimeter-size regions and may be lost from decimeter-size regions. Such a process would be expected to enrich the residual rock in ^{34}S. An extrapolation of these conclusions would be that S is lost by impact-vaporization from kilometer-size regions of large bodies. In fact, this appears to be the case for the lunar regolith. Lunar fines (especially fine-grained sieve samples) are enriched in δ^{34}S (Rees and Thode, 1974). Clayton et al. (1974) concluded that such an isotopic enrichment implied a loss of 20 to 30% of the original S abundance in the regolith. They proposed that micrometeorite bombardment and ion sputtering were responsible.

If impact-vaporization and loss of S could occur on the Moon (r = 1738 km), then it is also likely to occur on asteroids. This may be the case for asteroid 433 Eros (33 $\times$ 13 $\times$ 13 km). The NEAR-Shoemaker X-ray spectrometer (which has a sampling depth of $<$100 μm for the elements of interest) determined that Eros most likely has a primitive chondritic composition (Trombka et al., 2000), apparently similar to that of an LL chondrite (Chapman, 2001). Hence, Eros probably experi-

Table 3. Composition of the Smyer metal-sulfide nodule determined by INAA.[a]

Parameter	Na (mg/g)	Cr (mg/g)	Mn (mg/g)	Fe (mg/g)	Co (mg/g)	Ni (mg/g)	Cu (μg/g)	Ga (μg/g)	As (μg/g)	Se (μg/g)	Mo (μg/g)	Ru (μg/g)	Sb (ng/g)	W (μg/g)	Re (ng/g)	Os (μg/g)	Ir (μg/g)	Au (μg/g)
Nodule	0.024	1.07	0.036	870	3.65	77.4	480	19.7	9.29	37.5	5.65	5.12	308	0.615	320	3.80	3.54	1.04
Jilin Metal	ND	ND	ND	905	4.94	85.0	237	12.8	14.2	ND	3.96	6.65	492	0.86	350	3.54	3.20	1.28

[a] Mass of nodule = 26.17 mg. Jilin metal data from Kong et al. (1998).
ND = not determined.

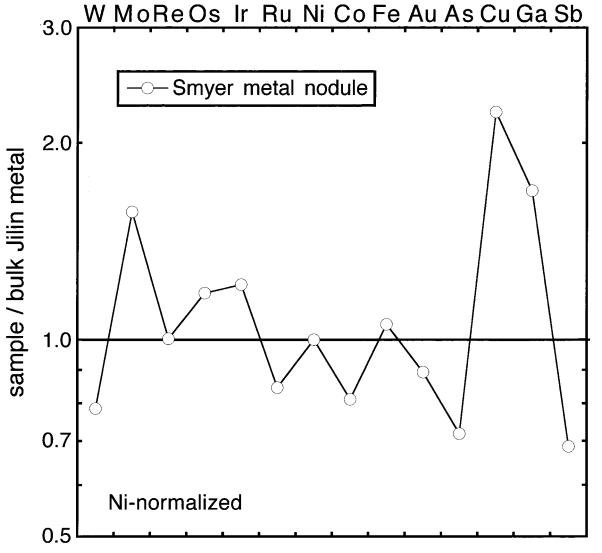

Fig. 9. Bulk composition of the metal-sulfide nodule in Smyer. Data are normalized to Ni and to bulk metal from the Jilin H5 chondrite (Kong et al., 1998). Elements are listed from left to right in order of decreasing volatility.

enced little or no partial melting; S is unlikely to have been sequestered in a metal-sulfide melt that drained toward the asteroid core.

Two portions of the surface of asteroid 433 Eros that were excited by energetic solar flares (Trombka et al., 2000) have S/Si weight ratios (0.036 ± 0.007 and 0.052 ± 0.006) that are much lower than those of mean H (0.116), L (0.113) and LL (0.111) chondrite falls (Jarosewich, 1990). I suggest that the low S at the surface of Eros results from volatilization and loss of S during impact events. Processes of S vaporization such as those documented for Smyer may have played a major role in depleting the surface of Eros and, presumably other chondritic asteroids, in S.

Acknowledgments—I thank S. Arnold for alerting me to the Smyer meteorite and for providing samples. I am grateful to G. W. Kallemeyn for performing the INAA on the Smyer metal nodule. I thank D. S. Lauretta for interesting discussions and for sending a copy of his dissertation to me. I also thank P. C. Buchanan, D. S. Lauretta, T. Kojima, and D. W. Mittlefehldt for helpful reviews. This work was supported in part by NASA grant NAG5-4766.

Associate editor: C. Koeberl

REFERENCES

Ashworth J. R. (1985) Transmission electron microscopy of L-group chondrites, 1. Natural shock effects. *Earth Planet. Sci. Lett.* **73,** 17–32.

Baedecker P. A. and Grossman J. N. (1989) *The Computer Analysis of High Resolution Gamma-Ray Spectra from Instrumental Neutron Activation Analysis Experiments.*Open File Report 89-454. U.S. Geological Survey.

Bennett M. E. and McSween H. Y. (1996) Shock features in iron–nickel metal and troilite of L-group ordinary chondrites. *Meteor. Planet. Sci.* **31,** 255–264.

Bogard D. D. (1979) Chronology of asteroid collisions as recorded in meteorites. In *Asteroids*(eds. T. Gehrels and M. S. Matthews), pp. 558–578. University of Arizona Press.

Bogard D. D., Garrison D. H., Norman M., Scott E. R. D., and Keil K. (1995) ^{39}Ar-^{40}Ar age and petrology of Chico: Large-scale impact melting on the L chondrite parent body. *Geochim. Cosmochim. Acta* **59,** 1383–1399.

Brandes E. A. and Brook G. B., eds. (1992) *Smithells Metals Reference Book,* 7th ed. Butterworth-Heinemann.

Brearley A. J. and Jones R. H. (1998) Chondritic meteorites. In *Reviews in Mineralogy* (ed. J. J. Papike), Vol. 36, pp. 3-1–3-398. Mineralogical Society of America.

Casanova I., Keil K., Wieler R., San Miguel A., and King E. A. (1990) Origin and history of chondrite regolith, fragmental and impact-melt breccias from Spain. *Meteoritics* **25,** 127–135.

Chapman C. R. (2001) Eros at very high resolution: Meteoritical implications (abstract). *Meteor. Planet. Sci.* **36**, A39–A40.

Chou C.-L. and Cohen A. J. (1973) Gallium and germanium in the metal and silicates of L- and LL-chondrites. *Geochim. Cosmochim. Acta* **37,** 315–327.

Clayton R. N., Mayeda T. K., and Hurd J. M. (1974) Loss of oxygen, silicon, sulfur, and potassium from the lunar regolith. *Proc. Lunar Sci. Conf.* **5,** 1801–1809.

de Bremond d'Ars J., Arndt N. T., and Hallot E. (2001) Analog experimental insights into the formation of magmatic sulfide deposits. *Earth Planet. Sci. Lett.* **186,** 371–381.

Dobson D. P., Crichton W. A., Vočadlo L., Jones A. P., Wang Y., Uchida T., Rivers M., Sutton S., and Brodholt J. P. (2000) In situ measurement of viscosity of liquids in the Fe-FeS system at high pressures and temperatures. *Am. Mineral.* **85,** 1838–1842.

Dodd R. T. (1981) *Meteorites—A Petrologic–Chemical Synthesis.* Cambridge University Press.

Dodd R. T. and Jarosewich E. (1979) Incipient melting in and shock classification of L-group chondrites. *Earth Planet. Sci. Lett.* **44,** 335–340.

Dodd R. T. and Jarosewich E. (1982) The compositions of incipient shock melts in L6 chondrites. *Earth Planet. Sci. Lett.* **59,** 355–363.

Fruland R. M. (1975) Volatile movement in the Rose City meteorite, and implications concerning the impact and late thermal history of ordinary chondrites (abstract). *Meteoritics* **10,** 403–404.

Gomes C. B. and Keil K. (1980) *Brazilian Stone Meteorites.* University of New Mexico Press.

Grady M. M. (2000) *Catalogue of Meteorites*, 5th ed. Cambridge University Press.

Jarosewich E. (1990) Chemical analyses of meteorites: A compilation of stony and iron meteorite analyses. *Meteoritics* **25,** 323–337.

Jurewicz A. J. G., Jones J. H., Weber E. T., and Mittlefehldt D. W. (1993) Partial melting of ordinary chondrites: Lost City (H) and St. Séverin (LL) (abstract). *Lunar Planet. Sci.* **24,** 739–740.

Keil K. (1962) Quantitativ erzmikroskopische Integrationsanalyse der Chondrite. *Chem. Erde.* **22,** 281–348.

King E. A. (1979) Smyer, Texas: A new clast-rich impact melt-breccia meteorite (abstract). *Meteoritics* **14,** 443.

Klöck W. (1986) Petrologische und geochemische Untersuchungen metallischen Eisens und koexistierender Silikate in terrestrischen Basalten. Ph.D. dissertation. Johannes-Gutenberg University, Mainz.

Kong P., Ebihara M., and Xie X. (1998) Reevaluation of formation of metal nodules in ordinary chondrites. *Meteorit. Planet. Sci.* **33,** 993–998.

Kring D. A., Swindle T. D., Britt D. T., and Grier J. A. (1996) Cat Mountain: A meteoritic sample of an impact-melted asteroid regolith. *J. Geophys. Res.* **101,** 29353–29371.

Lauretta D. S. (1997) Theoretical and experimental studies of iron–nickel–sulfur, beryllium, and boron cosmochemistry. Ph.D. thesis. Washington University, St. Louis.

Lauretta D. S., Lodders K., Fegley B., and Kremser D. T. (1997) The origin of sulfide-rimmed metal grains in ordinary chondrites. *Earth Planet. Sci. Lett.* **151,** 289–301.

Mason B. and Wiik H. B. (1966) The composition of the Bath, Frankfort, Kakangari, Rose City, and Tadjera meteorites. *Am. Museum Novitates* **2272,** 1–24.

Mason B. and Graham A. L. (1970) Minor and trace elements in meteoritic minerals. *Smithson. Contrib. Earth Sci.* **3,** 1–17.

McSween H. Y. (1999) *Meteorites and Their Parent Planets,* 2nd ed. Cambridge University Press.

Mittlefehldt D. W. and Lindstrom M. M. (2001) Petrology and geo-

chemistry of Patuxent Range 91501, a clast-poor impact melt from the L-chondrite parent body and Lewis Cliff 88663, an L7 chondrite. *Meteorit. Planet. Sci.* **36,** 439–457.

Miyamoto M., Takeda H., and Ishii T. (1984) Mineralogical comparison and cooling history of lunar and chondritic vesicular melt breccias. *J. Geophys. Res.* **89,** 11581–11588.

Olsen E. (1981) Vugs in ordinary chondrites. *Meteoritics* **16,** 45–59.

Rambaldi E. R. and Cendales M. (1979) Moderately volatile siderophiles in ordinary chondrites. *Earth Planet. Sci. Lett.* **44,** 397–408.

Rees C. E. and Thode H. G. (1974) Sulphur concentrations and isotope ratios in Apollo 16 and 17 samples (abstract). *Lunar Sci.* **5,** 621–623.

Rose L. A. and Brenan J. M. (2001) Wetting properties of Fe-Ni-Co-Cu-O-S melts against olivine: Implications for sulfide melt mobility. *Econ. Geol.* **96,** 145–157.

Rubin A. E. (1985) Impact melt products of chondritic material. *Rev. Geophys.* **23,** 277–300.

Rubin A. E. (1990) Kamacite and olivine in ordinary chondrites: Intergroup and intragroup relationships. *Geochim. Cosmochim. Acta* **54,** 1217–1232.

Rubin A. E. (1992) A shock-metamorphic model for silicate darkening and compositionally variable plagioclase in CK and ordinary chondrites. *Geochim. Cosmochim. Acta* **56,** 1705–1714.

Rubin A. E. (1995) Fractionation of refractory siderophile elements in metal from the Rose City meteorite. *Meteoritics* **30,** 412–417.

Rubin A. E. (1999) Formation of large metal nodules in ordinary chondrites. *J. Geophys. Res.* **104,** 30.,799–30, 804.

Rubin A. E., Sailer A. L., and Wasson J. T. (1999) Troilite in the chondrules of type-3 ordinary chondrites: Implications for chondrule formation. *Geochim. Cosmochim. Acta* **63,** 2281–2298.

Rubin A. E., Ulff-Møller F., Wasson J. T., and Carlson W. D. (2001a) The Portales Valley meteorite breccia: Evidence for impact-induced melting and metamorphism of an ordinary chondrite. *Geochim. Cosmochim. Acta* **65,** 323–342.

Rubin A. E., Zolensky M. E., and Bodnar R. J. (2001b) The halite-bearing Zag and Monahans (1998) meteorite breccias: Shock metamorphism, thermal metamorphism and aqueous alteration on the H-chondrite parent body. *Meteorit. Planet. Sci*., in press.

Sato G., Takeda H., Yanai K., and Kojima H. (1982) Electron microprobe study of impact-melted regolith breccias (abstract). In *Workshop on Lunar Breccias and Soils and Their Meteoritic Analogs* (eds. G. J. Taylor and L. L. Wilkening), pp. 120–122. LPI Technical Report 82-02. Lunar Planetary Institute.

Scott E. R. D. (1982) Origin of rapidly solidified metal–troilite grains in chondrites and iron meteorites. *Geochim. Cosmochim. Acta* **46,** 813–823.

Stöffler D., Keil K., and Scott E. R. D. (1991) Shock metamorphism of ordinary chondrites. *Geochim. Cosmochim. Acta* **55,** 3845–3867.

Takeda H., Huston T. J., and Lipschutz M. E. (1984) On the chondrite–achondrite transition: Mineralogy and chemistry of Yamato 74160 (LL7). *Earth Planet. Sci. Lett.* **71,** 329–339.

Taylor G. J., Keil K., Berkley J. L., and Lange D. E. (1979) The Shaw meteorite: History of a chondrite consisting of impact-melted and metamorphic lithologies. *Geochim. Cosmochim. Acta* **43,** 323–337.

Trombka J. I., Squyres S. W., Brückner J., Boynton W. V., Reedy R. C., McCoy T. J., Gorenstein P., Evans L. G., Arnold J. R., Starr R. D., Nittler L. R., Murphy M. E., Mikheeva I., McNutt R. L., McClanahan T. P., McCartney E., Goldsten J. O., Gold R. E., Floyd S. R., Clark P. E., Burbine T. H., Bhangoo J. S., Bailey H., and Petaev M. (2000) The elemental composition of asteroid 433 Eros: Results of the NEAR-Shoemaker x-ray spectrometer. *Science* **289,** 2101–2105.

Van Schmus W. R. and Ribbe P. H. (1968) The composition and structural state of feldspar from chondritic meteorites. *Geochim. Cosmochim. Acta* **32,** 1327–1342.

Weill D. F., Grieve R. A., McCallum I. S., and Bottinga Y. (1971) Mineralogy-petrology of lunar samples. Microprobe studies of samples 12021 and 12022; viscosity of melts of selected lunar compositions. *Proc. Lunar Sci. Conf.* **2,** 413–430.

Widom E., Rubin A. E., and Wasson J. T. (1986) Composition and formation of metal nodules and veins in ordinary chondrites. *Geochim. Cosmochim. Acta* **50,** 1989–1995.

Wilkening L. L. (1978) Tysnes Island: An unusual clast composed of solidified, immiscible, Fe-FeS and silicate melts. *Meteoritics* **13,** 1–9.

Willis J. and Wasson J. T. (1981) Instrumental neutron activation analysis of iron meteorites. *Radiochim. Acta* **29,** 45–51.

Yamaguchi A., Scott E. R. D., and Keil K. (1999) Origin of a unique impact-melt rock—The L-chondrite Ramsdorf. *Meteorit. Planet. Sci.* **34,** 49–59.